1-1-1981

Creep damage in the neighborhood of a hole in a tensile specimen.

Tai-Sheng Liu

CREEP DAMAGE IN THE NEIGHBORHOOD OF A HOLE IN A TENSILE SPECIMEN

by

Tai-Sheng Liu

A Thesis

Presented to the Graduate Committee

of Lehigh University

in Candidacy for the Degree of

Master of Science

in

Applied Mechanics

Lehigh University

1981

CERTIFICATE OF APPROVAL

This thesis is accepted and approved in partial fulfillment of the requirements for the degree of Master of Science.

10 December 1981
(date)

Professor in Charge

Chairman of the Department

ACKNOWLEDGEMENTS

The author wishes to express his sincere thanks to his advisor, Professor T.J. Delph, for his guidance, his kind encouragement and support in both financial and material aspects. The author also wishes to express his gratitude to Dr. R.J. Fields for his helpful consultation, his inspiration and kind assistance while working at the National Bureau of Standards, MD with him as a guest worker.

The author would like to give thanks to his dear parents, parents-in-law and his dearest wife for their endless encouragement and blessing.

The author would like to express his appreciation to Mrs. Donna Reiss for her help in typing the manuscript. Grateful acknowledgement is also made to the Department of Energy for partial support of the graduate studies of which this thesis is a part.

TABLE OF CONTENTS

LIST OF FIGURES

ABSTRACT

Qualitative comparisons between theoretical predictions based on finite element analysis and experimental results are made on the creep damage distribution in the neighborhood of a hole in the center of a 2 1/4 Cr-1 Mo stainless steel tensile specimen. Robinson's constitutive theory with instantaneous elastic responses as initial conditions is used to calculate the time dependent stresses and inelastic strains in the specimen. The uniaxial creep damage law suggested by Piatti et al. is then generalized to multiaxial stress states by employing two different models - one based on the maximum principal normal stress and the other on the Von Mises effective stress. Both theoretical predictions and experimental results show the greatest cavitation near the root of the hole, the area in which the stress concentration is highest.

I. INTRODUCTION

Creep is a kind of time-dependent inelastic strain that occurs when a material is subjected to a stress at elevated temperature for a prolonged period of time. The use of metallic materials under conditions where creep occurs may result in continuous accumulation of "creep damage" to the material. Such damage is one of the dominant failure modes in structures which must operate at very high temperatures for long periods of time, e.g., advanced nuclear reactors, coal gasification vessels, gas turbines and solar energy "power towers." Therefore, as energy conversion devices operate at increasingly higher temperatures, designers then must consider what amount of creep damage can be tolerated during the required service life.

As has been shown by Fields et al. [1], failure by creep rupture as a result of accumulated creep damage at elevated temperature may occur as a result of a number of different mechanisms. However, at stress levels of engineering interest, the dominant failure mechanism in metals is almost always that of intergranular cracking and fracture. This cracking is brought about by nucleation and growth of microscopic voids along the grain boundaries, which eventually coalesce with each other to form an array of microcracks leading to damage.

There are two principal ways of approaching the problem of estimating the time-to-failure of high-temperature components

under creep damage conditions. One is the phenomenological approach favored by workers in the mechanics of solids and the other is the microscopic approach pursued by materials scientists.

The most prominent example of the phenomenological approach to the prediction of creep rupture is the time-fraction rule which has been adopted for design use by the A.S.M.E. Boiler and Pressure Vessel Code [2]. It states that the creep damage, in general, is only a function of stress experienced by the material during the loading history. Due to its simplicity and the fact that other phenomenological failure criteria do not offer significantly better predictive capability, the time-fraction rule has been widely used in design applications.

In contrast to the phenomenological approach, the microscopic approach pursued by materials scientists has focused primarily upon the problem of describing the mechanisms responsible for the nucleation, growth, and coalescence of voids at grain boundaries. It is based on the materials science viewpoint that the void area fraction (or volume fraction) distribution present in a structural component at any given time constitutes a direct measure of the "creep damage" incurred by the component. Here the void area fraction is to be defined as the ratio of the grain boundary area covered by voids to the total grain boundary area. The aim here has consistently been to provide models for these phenomena which

would be capable, as a minimum, of explaining the experimentally observed variation in time-to-rupture with stress, temperature, grain size, etc., which have been observed in uniaxial tension tests. Some recent representative samples of this approach are the work of Chuang et al [3] and Chen [4]. However, to date, such models have not been developed to the point where they are felt to be useful for design purposes.

Traditionally, most of the experimental data relating to creep damage or creep rupture has been collected from uniaxial tension tests. Because of the experimental difficulties involved, relatively little data exists for multiaxial states of stress. In addition, there exists no universally accepted means of calculating creep damage in a multiaxial stress state from uniaxial stress data. However, elevated-temperature structural components typically contain complex multiaxial stress fields. The existence of multiaxial stresses is known to have a considerable influence upon creep rupture behavior, but, as noted, information concerning the precise nature of this influence is somewhat sketchy.

A considerable portion of this experimental evidence may be represented in a common form due to Hayhurst [5]. Hayhurst suggested that, under multiaxial states of stress, the uniaxial stress in creep damage models derived from uniaxial tensile tests should be replaced by a linear combination of the maximum principal normal stress, the Von Mises effective stress, and the hydrostatic

stress (first invariant of the stress tensor). The hydrostatic stress, however, has not been reported to have a great deal of influence upon creep damage behavior, and most experimental work to date has been interpreted in terms of maximum principal normal stress and/or the Von Mises effective stress.

The aims of our present study are to carry out creep damage calculations in the area of a stress concentration based on a void growth model obtained from density change measurements and to investigate two different multiaxial creep damage criteria - one governed by maximum principal normal stress versus one dependent upon the Von Mises effective stress. Finally we will compare these two criteria to experimental observations of cavitation in 2¼ Cr - 1 Mo specimens.

II. ANALYSIS

The particular problem to be analyzed is that of a flat tensile strip specimen with a hole in the center under creep conditions. We are particularly interested in calculating the creep damage around the hole. The effect of the central hole is to induce a multiaxial stress state into the tensile strip. As stated in the Introduction there exists no universally accepted means of calculating creep damage in a multiaxial stress state from uniaxial stress data. In the present work we will adopt the uniaxial creep damage law suggested by Piatti et al [6]. In Piatti's formulation the creep damage is taken to be a function of stress, inelastic strain, time and temperature. In [7] and [8] damage laws of this type have been determined for AISI 310 stainless steel and 2¼ Cr - 1 Mo stainless steel respectively by statistically analyzing the results of very precise density change measurements made on specimens tested under constant-load tension for a range of temperatures. The ratio of the change in density to the original density, $\Delta\rho/\rho_o$, was taken as a direct measure of the amount of creep damage present in the material at a given time, since it may presumably be related directly to the void volume fraction.

A fairly involved statistical analysis revealed that for both 2¼ Cr - 1 Mo and AISI 310 stainless steel, the density change data were best fit by the following relation

$$D = -\frac{\Delta\rho}{\rho_o} = H\,\varepsilon^{\alpha}\, e^{-\frac{\beta}{T}}\, \sigma_o^{\gamma}\, t^{\delta} \qquad (2.1)$$

where D is the damage (density change normalized by the original density) produced by the initial stress σ_o and the inelastic strain ε at the reference temperature T in the time t. Here α, β, γ and δ are material constants at a given temperature. Equation (2.1) can be written as

$$\frac{d}{dt}\left[\frac{D}{H_o \varepsilon^{\alpha}}\right]^{1/\delta} = \sigma_o^{\gamma/\delta} \qquad (2.2)$$

where $H_o = He^{-\frac{\beta}{T_o}}$. Equation (2.2) then is completely equivalent to (2.1) for σ_o constant with time.

In generalizing equation (2.2) to the case of variable stress σ, Piatti et al [6] postulated that the damage rate be a function of axial inelastic strain, stress, damage and axial inelastic strain rate, i.e.

$$\dot{D} = \dot{D}(\varepsilon, \sigma, D, \dot{\varepsilon})$$

where

$$\frac{d}{dt}(\dot{\ }) = (\dot{\ })$$

They replaced σ_o in (2.2) by σ and integrated stress over the whole time history to obtain the following incremental damage law, which is the uniaxial damage law we will adopt in the present work

$$D = -\frac{\Delta\rho}{\rho_o} = H\varepsilon^{\alpha}\left[\int_0^t \sigma^{\gamma/\delta}\, d\tau\right]^{\delta} \qquad (2.3)$$

where the constants H, α, γ and δ are given for $2\frac{1}{4}$ Cr - 1 Mo in [8] for a range of temperatures. The temperature of interest in the present case was 565° C (1049°F), and values of H, α, γ and δ for this temperature were obtained by linear interpolation from tabular data presented in [8].

The values obtained for each constant are, for ε expressed in percent

$$H = e^{-17.33},\ \alpha = 0.47,\ \gamma = 3.76,\ \delta = 0.33\ .$$

Substituting these values into equation (2.3) and converting strain to the usual, non-percentage measure, we have

$$D = 2.592\times10^{-7}(\varepsilon^I)^{0.47}\left[\int_0^t \sigma^{11.39}\, d\tau\right]^{0.33} \qquad (2.4)$$

Since equation (2.4) is based on uniaxial analysis, we want to generalize it to a multiaxial stress state. We will consider two different ways of accomplishing this, one based on the maximum principal normal stress and inelastic strain, the other based on the Von Mises effective stress and inelastic strain. These two cases represent the limiting cases of the multiaxial generalization proposed by Hayhurst [5], assuming that the hydrostatic stresses have no influence upon void growth.

A. Maximum Principal Normal Stress Approach

This damage law is simply derived by substituting the maximum principal normal stress and inelastic strain, σ_{max} and ε^{I}_{max}, for the corresponding uniaxial quantities in the equation (2.4). It has the form

$$D = (2.592\times10^{-7})(\varepsilon^{I}_{max})^{0.47}\left[\int_{o}^{t} \sigma_{max}^{11.39}\, d\tau\right]^{0.33} \qquad (2.5)$$

From Mohr's circle under plane stress conditions, the maximum principal normal stresses and inelastic strains are given by

$$\sigma_{max} = \frac{(\sigma_{xx}+\sigma_{yy})}{2} + \left[\left(\frac{\sigma_{xx}-\sigma_{yy}}{2}\right)^2 + \sigma_{xy}^2\right]^{\frac{1}{2}}$$

$$\varepsilon^{I}_{max} = \frac{(\varepsilon^{I}_{xx}+\varepsilon^{I}_{yy})}{2} + \left[\left(\frac{\varepsilon^{I}_{xx}-\varepsilon^{I}_{yy}}{2}\right)^2 + (\varepsilon^{I}_{xy})^2\right]^{\frac{1}{2}}$$

where σ_{xx}, σ_{yy} and σ_{xy} are in-plane components of the stress tensor and ε^{I}_{xx}, ε^{I}_{yy} and ε^{I}_{xy} are in-plane components of the inelastic strain.

Negative maximum principal normal stresses were taken to be non-damaging in accordance with the belief that void growth is brought about only by tensile stresses.

B. Von Mises Effective Stress Approach

Here the damage law has the form

$$D = (2.592 \times 10^{-7})\bar{\varepsilon}^{0.47}\left[\int_0^t \bar{\sigma}^{11.39}\, d\tau\right]^{0.33} \qquad (2.6)$$

where

$$\bar{\varepsilon}^I = \left(\frac{2}{3}\varepsilon^I_{ij}\varepsilon^I_{ij}\right)^{\frac{1}{2}} = \left\{\frac{2}{3}\left[(\varepsilon^I_{xx})^2 + (\varepsilon^I_{yy})^2 + 2(\varepsilon^I_{xy})^2 + (\varepsilon^I_{zz})^2\right]\right\}^{\frac{1}{2}}$$

and

$$\varepsilon^I_{zz} = -(\varepsilon^I_{xx} + \varepsilon^I_{yy})$$

since the inelastic strains are assumed to be incompressible. The Von Mises effective stress is given by

$$\bar{\sigma} = (\sigma^2_{xx} + \sigma^2_{yy} - \sigma_{xx}\sigma_{yy} + 3\,\sigma^2_{xy})^{\frac{1}{2}}$$

Before we calculate creep damage according to the damage law suggested by Piatti et al [6], we have to know first how to obtain the time dependent stresses and inelastic strains. In the present work we'll use Robinson's constitutive theory [9] to calculate those two quantities. The principal advantage possessed by Robinson's model over the conventional representation is its ability to describe both short-term (plastic) behavior and long-term (creep) inelastic behavior with equal facility. In the conventional consideration, the inelastic strain is taken as the sum of a time-independent component which is given by the laws of

classical plasticity, and a time - dependent component which is given by some appropriate creep law. In contrast, Robinson's constitutive theory treats the inelastic strain as a completely time-dependent quantity without a time-independent component. It is known as a "state-variable theory" from its use of a variable of state in the governing equation or as a "unified theory" from its ability to model both short-term (plastic) behavior and long-term (creep) behavior.

For the loading history of our work, the governing equations for Robinson's theory are given in general multiaxial form in [9] and have the following forms:

$$2\mu\, \dot{\varepsilon}^{I}_{ij} = F^{\frac{n-1}{2}}\, \Sigma_{ij} \tag{2.7}$$

$$\dot{\gamma}_{ij} = \frac{2\mu T}{G^{\beta/2}}\, \dot{\varepsilon}^{I}_{ij} - R\, G^{\frac{m-\beta-1}{2}}\, \gamma_{ij} \tag{2.8}$$

where

$$F = \frac{J_2}{\kappa^2} - 1$$

$$J_2 = \frac{1}{2}\, \Sigma_{ij}\, \Sigma_{ij}$$

$$\Sigma_{ij} = S_{ij} - \gamma_{ij}$$

$$S_{ij} = \sigma_{ij} - \frac{1}{3}\, \sigma_{kk}\, \delta_{ij}$$

$$G = \frac{J_{12}}{\kappa^2}$$

$$J_{12} = \frac{1}{2} \gamma_{ij} \gamma_{ij}$$

$$\frac{d}{dt}( ) = \dot{( )}$$

The quantities μ, n, T, R, m, ξ and κ in these equations are material constants. ϵ^I_{ij} and γ_{ij} are the inelastic strain and state variable tensors, respectively. We will make use of some recently published values of the constants for Robinson's theory [10] which are derived from curve fits to constant stress creep and constant strain rate loading data for a particular heat of 2¼ Cr - 1 Mo stainless steel at 566°C (1050°F). The reported values are: $\mu = 1.061 \times 10^8$ MPa-hr, $n = 6.25$, $T = 3.0 \times 10^{-4}$ hr^{-1}, $R = 2.25 \times 10^{-5}$ hr^{-1}, $m = 4.50$, $\xi = 1.00$ and $\kappa = 6.895$ MPa.

We use Galerkin's technique to set up our finite element formulation of Robinson's time-dependent constitutive equations. Since our problem is a plane stress problem and our 2¼ Cr - 1 Mo experimental specimen is symmetric, we need only to analyze one-quarter of the specimen. The configuration of our one-quarter specimen, divided into 10 elements, is shown in Figure 1. We choose the 12-node isoparametric quadrilateral element (QUAD-12

element) to analyze our problem.

The equilibrium equation is

$$\sigma_{ij,j} + F_i = 0 \tag{2.9}$$

where σ_{ij} is the stress tensor, F_i is the $i^{\underline{th}}$ component of body force vector and $\frac{\partial}{\partial x_j}( ) \equiv ( )_{,j}$. In the displacement-based finite element method, we take

$$\{u\} = [N]\{\delta\}$$

where $\{u\}$ is the displacement array, $[N]$ is the interpolation function matrix and $\{\delta\}$ is the vector containing the displacements at the nodal points. The Galerkin's method gives

$$\int_V [N]^T(\{\sigma_{ij,j}\} + \{F_i\})dV = 0 \tag{2.10}$$

where $[N]^T$ is the transpose of $[N]$ and the integration is carried out over the whole volume of the specimen. For the plane stress problem, we take

$$dV = hdA$$

where h is thickness of the specimen. By applying the divergence theorem and making use of the symmetry of the stress tensor, we obtain

$$\int_A [B]^T\{\sigma\}dA = \oint_C [N]^T\{T\}dC + \int_A [N]^T\{F\}dA$$

where [B] is the strain-displacement matrix and {T} the vector of nodal point loads. Let $\{\varepsilon\}$ be the total strain due to all causes, $\{\varepsilon\}^E$ be the elastic strain and $\{\varepsilon\}^I$ be strains due to all other causes (in particular, inelastic strain). Now

$$\{\varepsilon\} = \{\varepsilon\}^E + \{\varepsilon\}^I$$

and from Hooke's law

$$\{\sigma\} = [C]\{\varepsilon\}^E = [C](\{\varepsilon\}-\{\varepsilon\}^I) = [C]([B]\{\delta\}-\{\varepsilon\}^I) \qquad (2.11)$$

where

$$[C] = \frac{E}{1-\nu^2}\begin{bmatrix} 1 & \nu & 0 \\ \nu & 1 & 0 \\ 0 & 0 & \frac{1-\nu}{2} \end{bmatrix}$$

Finally, for plane stress, substitution gives

$$\int_A [B]^T[C][B]dA\{\delta\} = \int_A [B]^T[C]\{\varepsilon\}^I dA + \oint_C [N]^T\{T\}dC + \int_A [N]^T\{F\}dA \qquad (2.12)$$

In the notation of the finite element method, we have

$$[k]\{\delta\} = \{F\} \qquad (2.13)$$

where $[k] = \int_A [B]^T[C][B]dA$ is the elastic stiffness matrix and

$$\{F\} = \int_A [B]^T[C]\{\varepsilon\}^I dA + \oint_C [N]^T\{T\}dC + \int_A [N]^T\{F\}dA$$

Thus we can write

$$\{\delta\} = [k]^{-1} \{F\} \tag{2.14}$$

where now $\{\epsilon\}^I$ are the time-dependent components of inelastic strain.

Equations (2.7) and (2.8) are first-order ordinary differential equations which give the inelastic strain and state variable rates as functions of the current values of the deviatoric stress and state variable tensors. The current values of the stresses may be found by solving the finite element equations (2.11) and (2.14). Equations (2.7) and (2.8) may be integrated forward in time from a given set of initial conditions. In the present work, we consider a step loading instantaneously applied at t=0, so that the initial stress distribution is found by solving the purely elastic finite element problem with $\{\epsilon\}^I = 0$. Robinson's constitutive equations are found to be relatively insensitive to the initial value of the state variable, so long as these are sufficiently small with regard to the steady-state values. Accordingly we take here as initial values $\gamma_{xx} = -0.01$ MPa, $\gamma_{yy} = 0.01$ MPa and $\gamma_{xy} = 0$. To solve these two ordinary differential equations (2.7) and (2.8), we first use the second-order modified Euler Predictor-Corrector integration scheme [11] to get five starting values for ϵ^I_{ij} and γ_{ij}. Then we use the fourth-order Adams-Bashforth-Moulton scheme [11] with automatic integration

step size control carry out the remainder of the integration. We use the Gaussian 3 x 3 integration formula [12] to evaluate all integrals in equation (2.12).

As noted, we substitute the inelastic strains ϵ_{ij}^{I} into equation (2.12) and use the finite element scheme to solve for $\{\delta\}$, the nodal point displacements. Then we substitute $\{\delta\}$ into equation (2.11), Hooke's law, to find the stresses $\{\sigma\}$.

In our work, the 2¼ Cr - 1 Mo stainless steel was loaded with a constant tensile load of 42 MPa at 565°C (1049°F) for 3000 hours; the load was then raised to 87.5 MPa for an additional 1324 hours. The load history is shown in Fig. 2. From time t=0 to t=3000 hrs, we calculate the stresses, inelastic strains and values of the state variables for each Gauss point inside the specimen by solving an initial value problem with the initial conditions mentioned previously. From time t=3000 to t=4324 hrs, we simply used the values of inelastic strain and state variable at t=3000 hrs as our initial conditions and modified the load vector (right-hand side vector) to the higher stress level, and then solve this new initial value problem. The eventual results of the analysis are the stress distributions at each time step and the values of inelastic strain at time t=4324 hrs. Those values are exactly what we want to calculate the creep damage distribution according to damage law, equations (2.5) and (2.6).

In using Piatti's damage law we employ the two limiting criteria discussed earlier - maximum principal normal stress approach and Von Mises effective stress approach - to evaluate creep damage for multiaxial stress state. In both cases, we use a simple trapezoidal integration rule to evaluate the integral in equations (2.5) and (2.6).

The values of creep damage are calculated at each Gauss point inside the element, not at each nodal point. In order to get the damage distribution of the nodal points, for the purposes of drawing contour plots, we will adopt the smoothing technique suggested by Hinton and Campbell [13].

We have calculated the values of the creep damage D at nine Gauss points in the interior of each element. Following the technique of [13], we define an approximate damage distribution over a given element by

$$\tilde{D}(x,y) = \sum_{i=1}^{12} N_i(x,y)\tilde{D}_i \qquad (2.15)$$

where the $N_i(x,y)$ are the interpolating functions for the QUAD-12 element and $\tilde{D}_i$ are the nodal point values for the approximate distribution. We define an error measure as

$$e(x,y) = D(x,y) - \tilde{D}(x,y) \qquad (2.16)$$

Take $\chi = \iint_A e^2(x,y)dx\,dy$ where here we sum up contributions from

every element in the area A. We then seek to minimize the square of the error by

$$\frac{\partial \chi}{\partial \tilde{D}_i} = 0 \tag{2.17}$$

This leads to the following finite element equations

$$[k_{ij}]\{\tilde{D}_i\} = \{R_i\} \tag{2.18}$$

where $$[k_{ij}]^e = \int_{-1}^{1}\int_{-1}^{1} N_i(r,s)N_j(r,s)|J|drds$$

$$\{R_i\}^e = \int_{-1}^{1}\int_{-1}^{1} N_i(r,s)D(r,s)|J|drds$$

and $[\ ]^e$ denotes the contribution from each element. Here r and s are the usual local coordinates for the quadrilateral element. In $\{R_i\}^e$, $D(r,s)$ are nine known creep damage values at the Gauss points. Hence we use Gaussian 3 x 3 integration formula to evaluate the right-hand side vector $\{R_i\}^e$ for each element. But in evaluating the coefficient matrix $[k_{ij}]^e$, we use a Gaussian 4 x 4 integration formula. The reason for using a higher order integration formula here is that a 3 x 3 integration scheme leads to a singular coefficient matrix.

The nodal point values obtained by this smoothing technique were then used to construct contour plots for the damage distribution. The results will be discussed in section IV.

III. EXPERIMENT

In our work we used two specimens fabricated from a commercial heat (Lukens heat C7158, ASTM A542-72, class 2) of 2¼ Cr - 1 Mo. They are shown with dimensions in Fig. 3. The heat treatment of these two specimens was done at National Bureau of Standards (NBS), and duplicated the heat treatment used in the study of Piatti et al [8]. The heat treatment procedures are as follows: 10 minutes at 1000°C, then cooled to 710°C at 35°C/hr, followed by 2 hours at 710°C, and finally cooled in the furnace to room temperature at 50°C/hr.

After the above heat treatment, the average grain diameter was found to be 40.4 μm which compares very favorably with the value reported in [8]. The resulting microstructure was the ferrite-pearlite structure shown in Fig. 4. A similar structure was reported in [8]. We see from Figure 4 that the pearlite colonies (dark grains) tend to be small while the ferrite grains (light grains) are larger. Figure 5 was taken at higher magnifications and indicate that the grain boundaries contain large numbers of carbides (Cr-Mo dual carbides). There are also some carbide precipitates within the grains. This is a very stable structure for the temperatures at 600°C and below.

In performing our creep experiments, we used two SATEC M-2 creep machines to load the specimens with a constant load at

temperature of 565°C. Thermocouples were attached to the specimens by spot welding them to a location about 1 cm above the top of the central hole. These were used to control the temperature. The loading history for both specimens are different and are shown in Fig. 2.

Specimen No.1 was crept at σ = 40 MPa for 4520 hours, then the load was increased to σ = 114 MPa for an additional 196 hours until failure occurred. Here σ is the nominal stress calculated by dividing the load by the undeformed specimen cross-sectional area, excluding the presence of the central hole.

Specimen No.2 was crept at σ = 42 MPa for 3000 hrs, and then rapidly air-cooled down to room temperature in the furnace and unloaded. It was sent to the National Bureau of Standards (NBS) for metallographic analysis, but no voids were observed. The specimen was then reloaded to σ = 87.4 MPa at the same temperature as before. We terminated this test after an additional 1324 hours.

After termination of both tests, the two specimens were sent to NBS for metallographic analysis. The results of the analyses will be discussed in the next section.

IV. RESULTS AND DISCUSSION

A. Finite Element Analysis

We used finite element codes to calculate creep damage distribution by employing two different models - one based primarily on the maximum principal normal stress, the other on the Von Mises effective stress. The creep damage distributions are normalized to be unity and plotted as contours over elements 1-6. They are shown for the maximum principal normal stress model and the Von Mises effective stress model in Fig. 6 and 7, respectively.

We see from Fig. 6 and Fig. 7 that there exists little qualitative difference between the predictions of the two models. This fact is, perhaps, not what might be expected. We also conclude from Fig. 6 and Fig. 7 that the creep damage distribution is much more severe in the neighborhood of the central hole rather than in the end of the specimen. Especially, it is most severe around the root of the hole which is the area of greatest stress concentration. This is, of course, what would be expected.

B. Experimental Results

First of all, it should be noted that only qualitative comparisons between the results of the experiments and the

finite element analysis are possible. This is the case because in calculating the creep damage distribution we used Robinson's constitutive theory equations (2.7) and (2.8) to obtain the time-dependent stresses and inelastic strains. The constants in these equations we adapted are those derived from curve fits to constant stress creep and constant strain rate loading data for a particular heat of 2 1/4 Cr-1 Mo stainless steel at 566°C (1050°F), as given in [10]. However, our 2 1/4 Cr-1 Mo specimens are fabricated from a different heat and have a different heat treatment than those Robinson used in [10]. Thus, we can expect quantitative differences to exist between the inelastic behavior of our specimens and those used by Robinson. Also, we mention that in our creep damage calculations according to equation (2.3) we used linear interpolation from tabular data presented in [8] to obtain the constants H, α, γ and δ. But H is actually an exponential function and we linearly interpolated its exponent. This might also lead errors to the creep damage calculations. Thus, only qualitative comparisons between analysis and experiment are valid here. We now turn to a discussion of the experimental results.

B.1 Experimental Results for Specimen No. 1 (Fractured)

The neighborhood around the central hole for the upper part of the fractured specimen No. 1 is shown in Fig. 8 with

the tensile axis parallel to the short axis of the photography. The fractured specimen is shown as the white part while the dark part is the background. We see from Fig. 8 that there is extensive cavitation (small dark spots in the white specimen background) at the area of greatest stress concentration near the hole. This can be seen clearly from Fig. 9 (a) and (b) which were taken with higher magnification around the stress concentration with tensile axis in the vertical direction of the photography. Fig. 9a was taken from left of Fig. 8, while Fig. 9b is from the right part.

It can be seen that specimen No.1 failed by a creep crack propagating from the edge of the hole (point of the highest stress concentration) outward. At the beginning the failure was due to intergranular cracking, and finally followed by rapid transgranular failure due to fast increased stresses on the crack tip. This can be seen from Fig. 10, 11 and 12 (all of them have their tensile axes in the vertical directions). Fig. 10 was taken near the central hole, the dark spots were cavities and were on the grain boundaries. Also note that cavities were opened by plastic deformation as fracture surface was approached. Fig. 11 was at higher magnification for the intergranular cavities near the central hole. Fig. 12 was taken near the edge of the specimen No. 1. Note the existence

of transgranular cavities across the grains. This is because the higher and rapidly increasing stress concentration on the crack tip led to cavities which did not have time to form along the grain boundaries.

B.2 Experimental Results for Specimen No. 2 (unfractured)

In specimen No. 2 we also find the heaviest cavitation in the neighborhood of stress concentration, as in specimen No. 1. This can be seen from Fig. 13. In Fig. 13, (a) and (b) are taken from the left and right parts of the unfractured specimen No. 2, respectively. The tensile axis is along the vertical direction.

We also find that all the cavitation in the neighborhood of the central hole appears to be intergranular in nature, whereas far away from the central hole there is no apparent cavitation. Intergranular cavities near the hole are shown in Fig. 14 which was taken at higher magnification in the area shown by Fig. 13(b). Figure 15 shows an area of the specimen away from the hole. We note no cavitation in this area.

These observations are in qualitative agreement with the results of the finite element analysis.

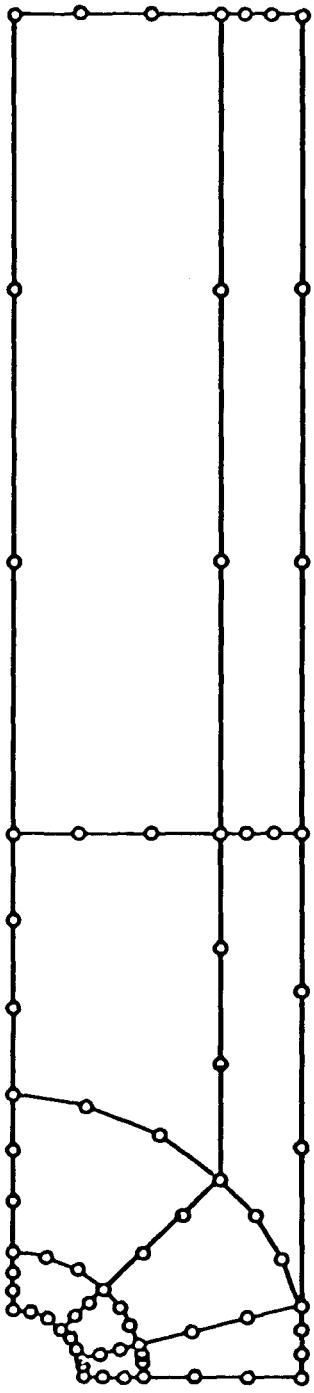

Fig. 1 Finite element configuration of right-upper quarter of 2 1/4 Cr-1 Mo tensile specimen (Top view).

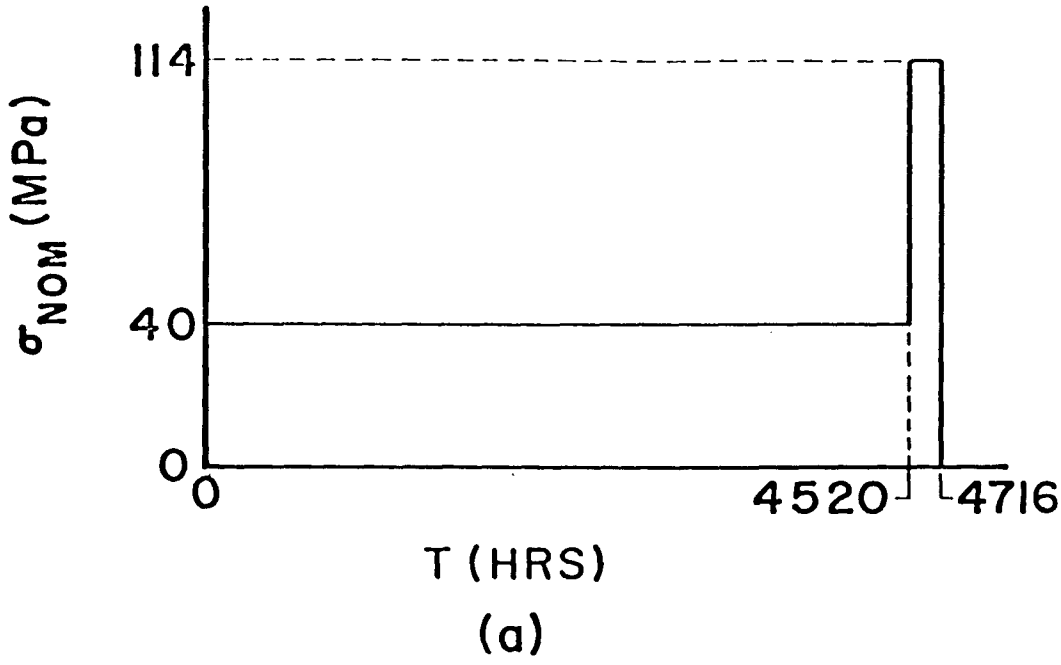

Fig. 2(a) Load history for specimen No. 1.

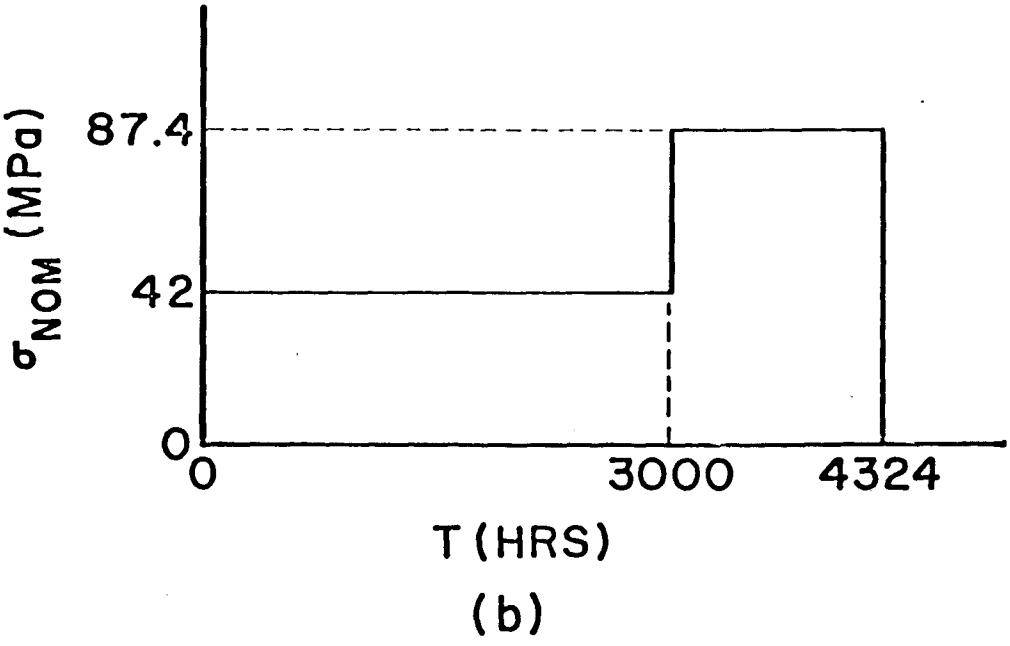

Fig. 2 (b) Load history for specimen No. 2.

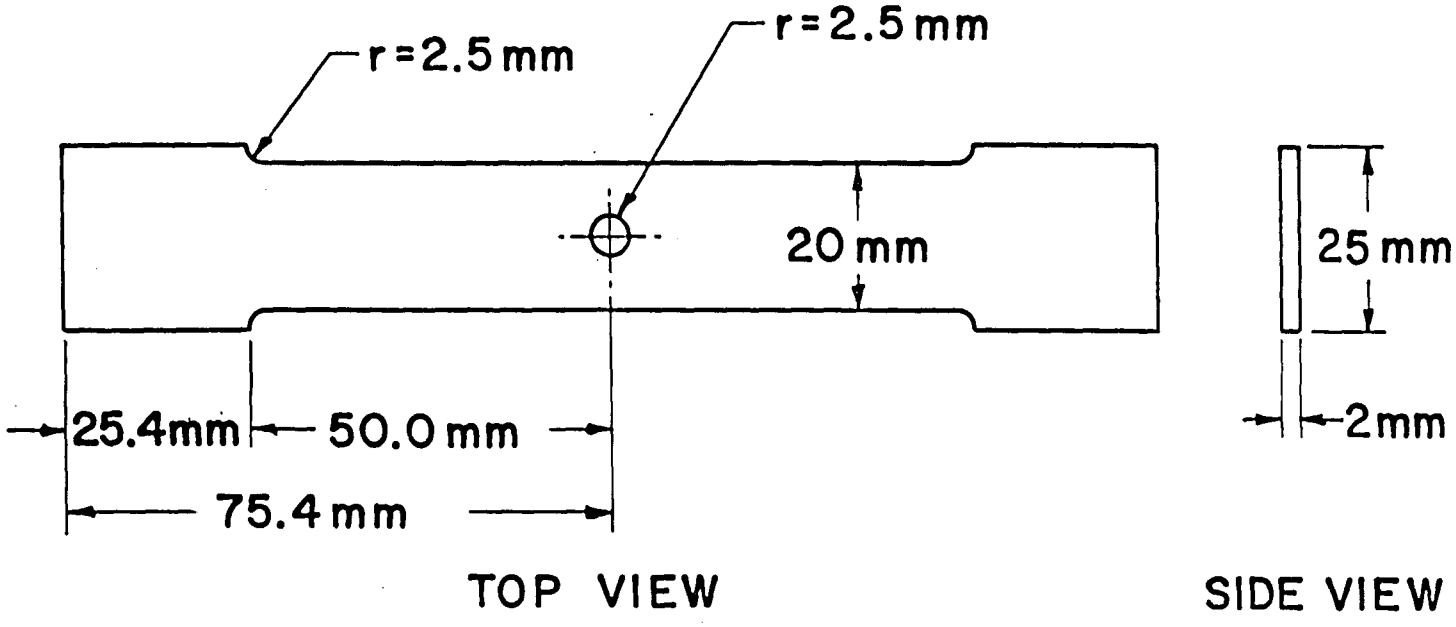

Fig. 3 Dimensions for 2 1/4 Cr-1 Mo tensile specimens.

Fig. 4 Microstructure of 2 1/4 Cr-1 Mo tensile specimen (Lukens heat C7158, ASTM A542-72, Class 2) after the heat treatment used in [8] [80X].

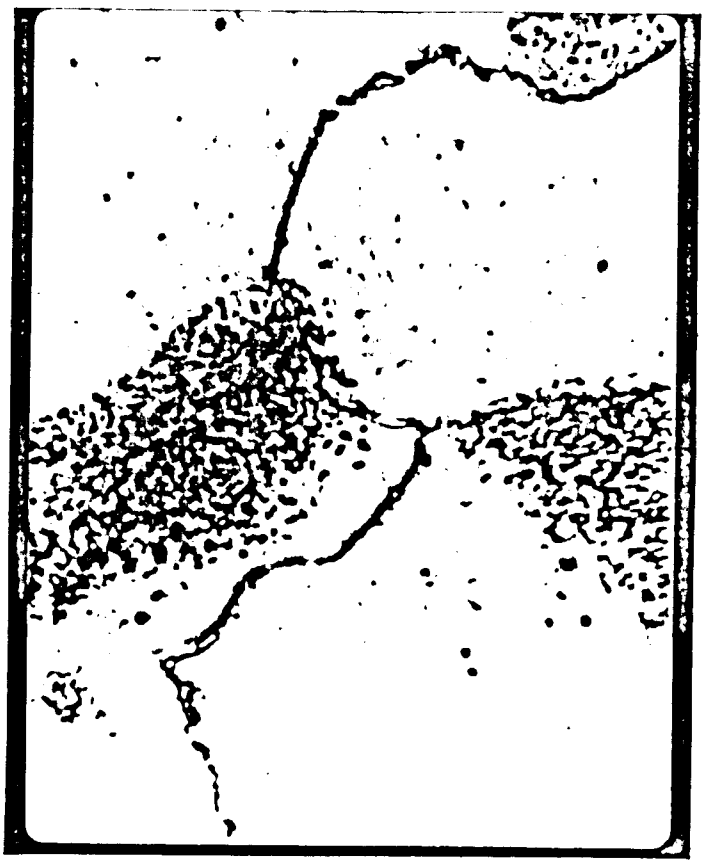

Fig. 5 Higher magnification of Fig. 4 [2500X].

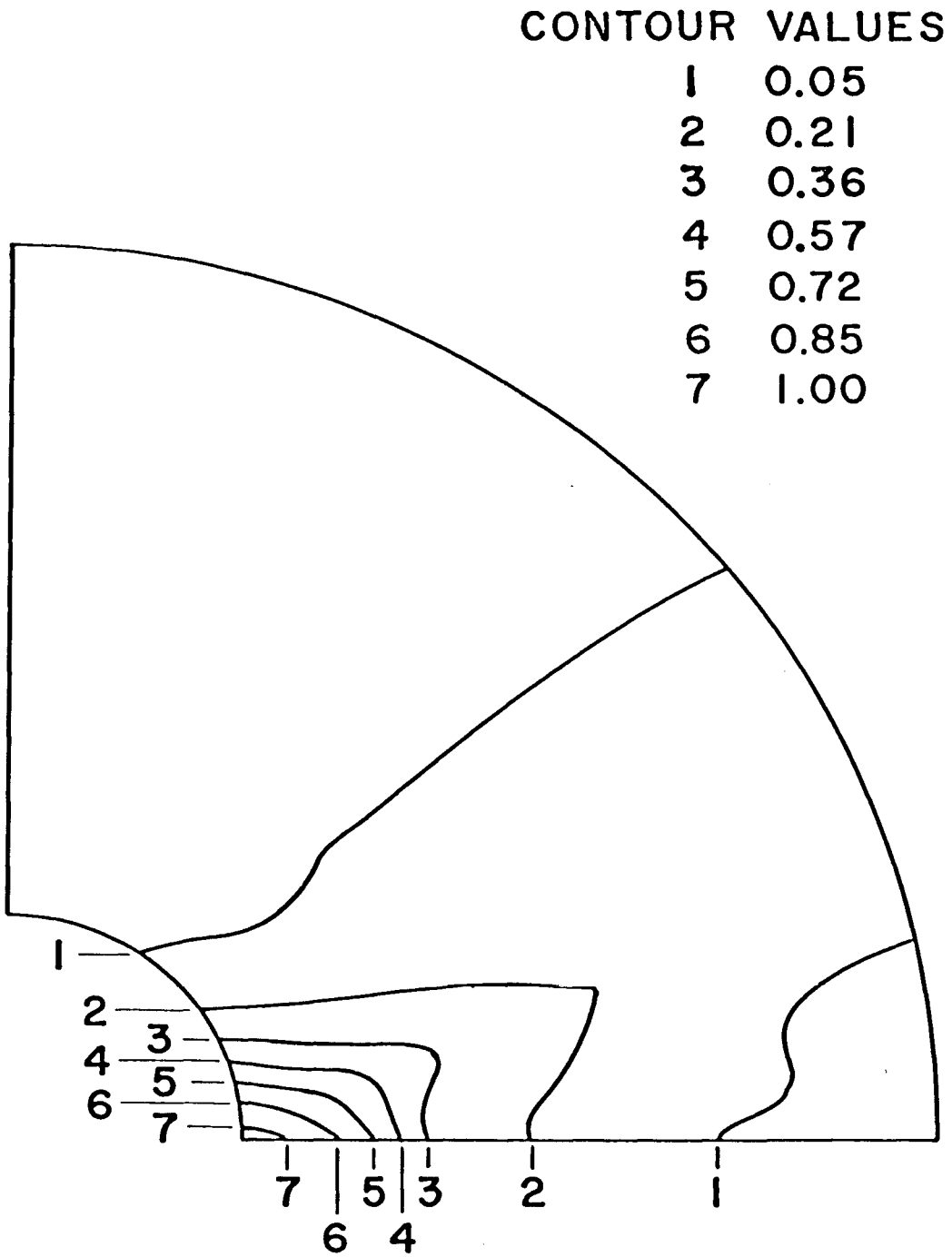

Fig. 6 Creep damage distribution contours over element 1-6 for the maximum principal normal stress model.

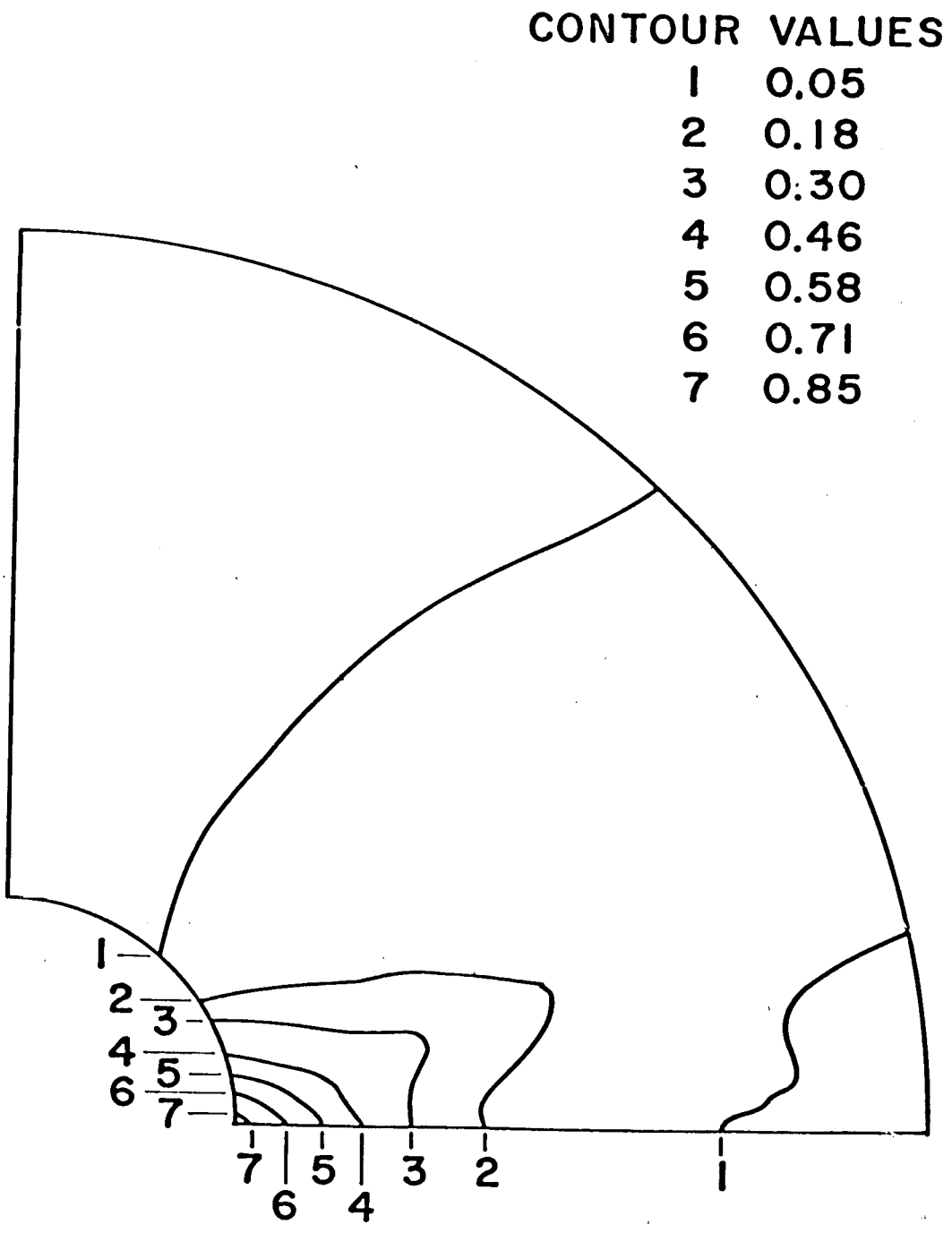

Fig. 7 Creep damage distribution contours over element 1-6 for the Von Mises effective stress model.

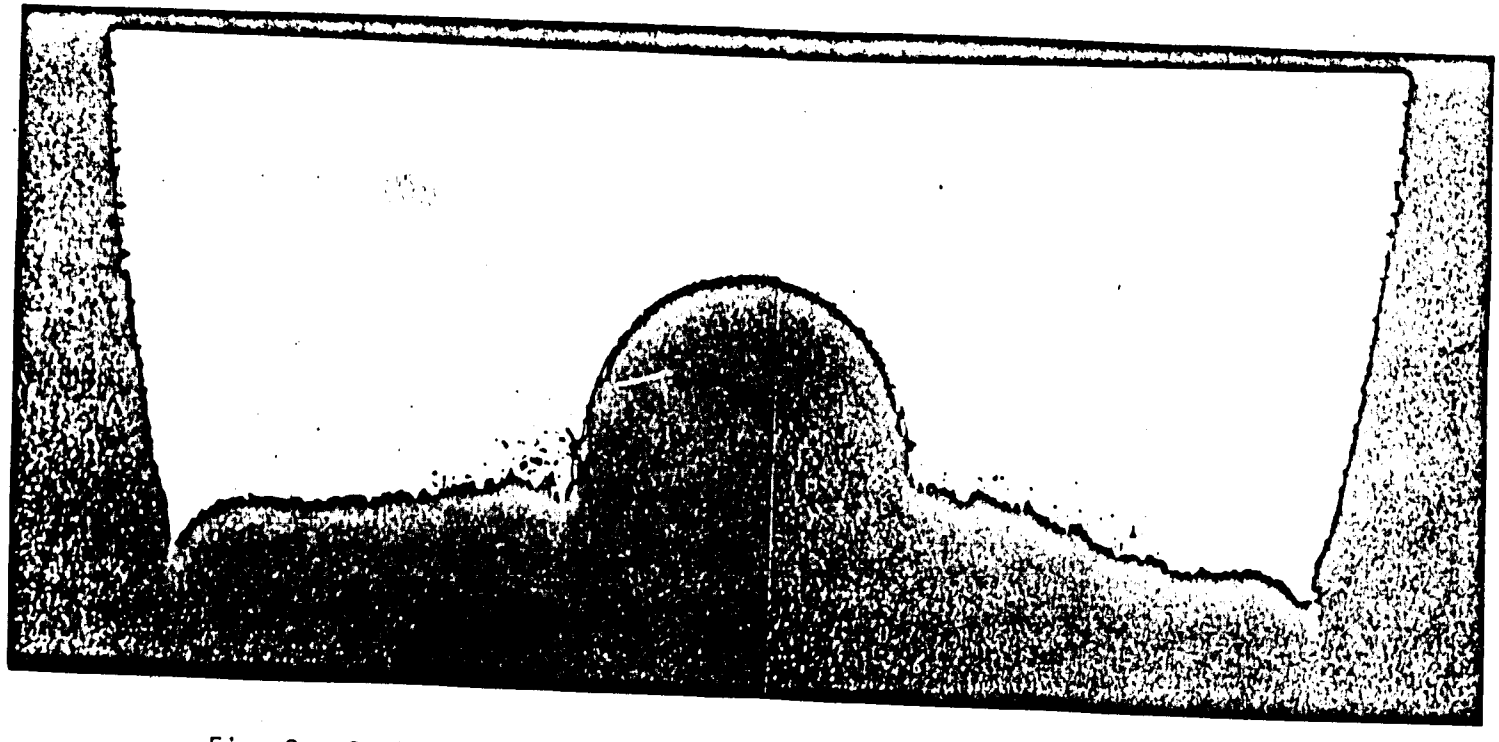

Fig. 8 Cavitation distribution over fracture specimen No. 1 [9 1/2 X].

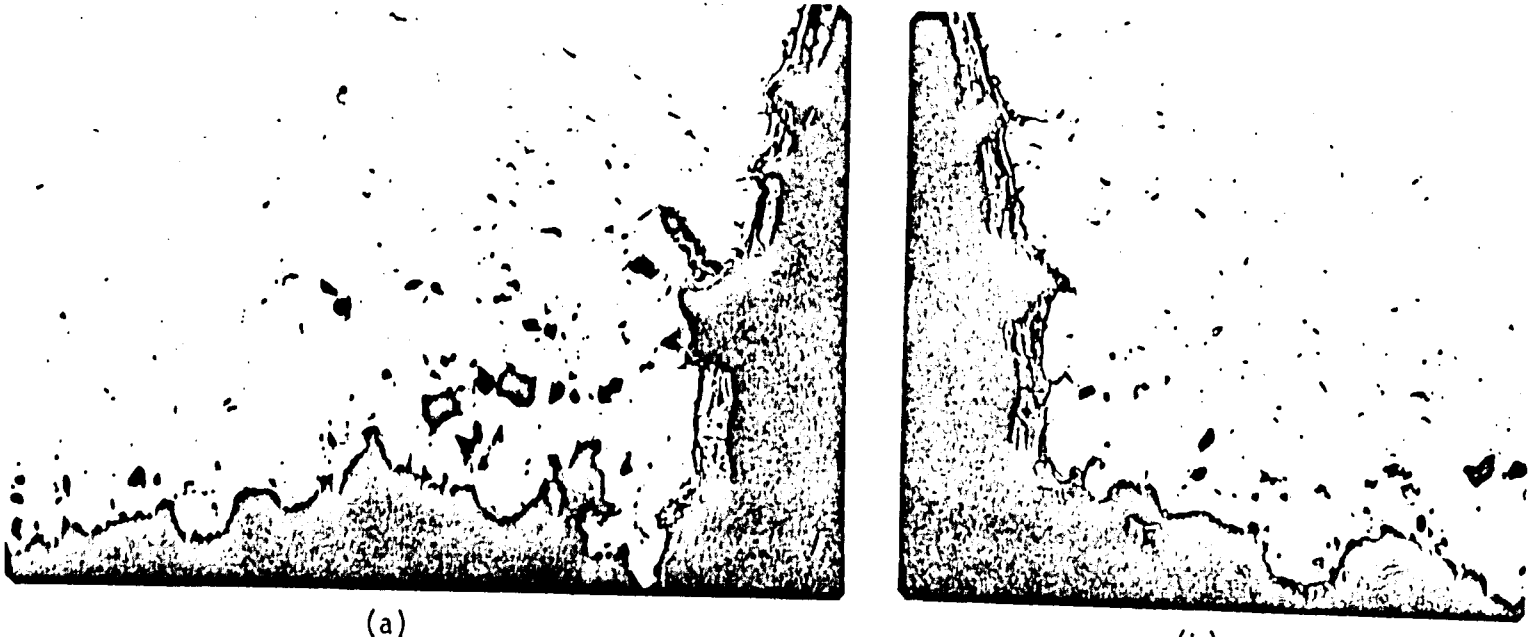

(a)

Left-hand side neighborhood of stress concentration of Fig. 8 [50X].

(b)

Right-hand side neighborhood of stress concentration of Fig. 8 [50X].

Fig. 9 Magnified cavitation distribution over fractured specimen No. 1.

Fig. 10 Etched intergranular cavities along the grain boundaries near the central hole of the fractured specimen No. 1 [112X, longitudinal section].

Fig. 11 Etched intergranular cavities along the grain boundaries near the central hole of the fractured specimen No. 1 [400X, longitudinal section].

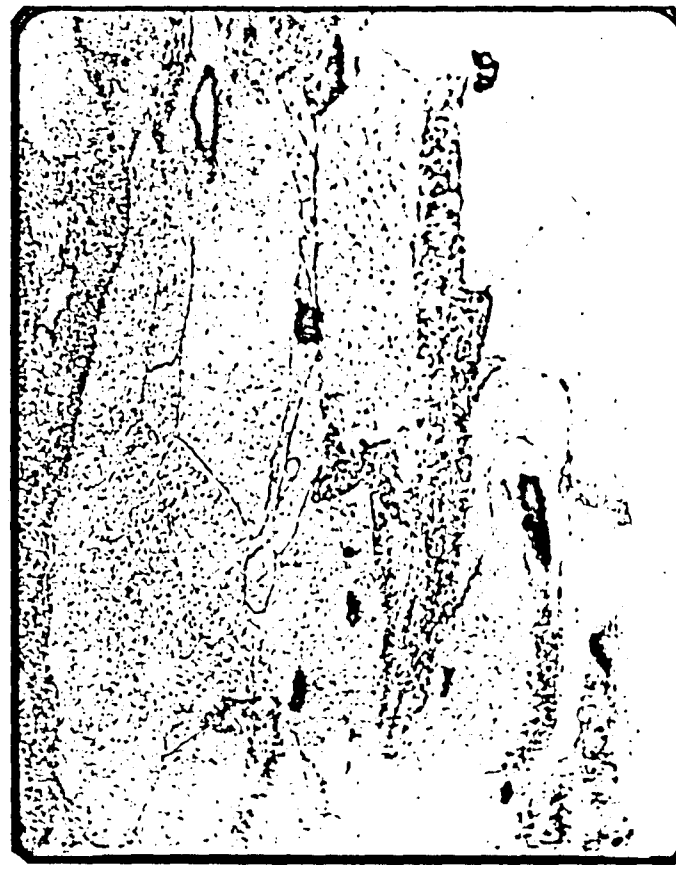

Fig. 12 Etched transgranular cavities across the grains near the edge of the fractured specimen No. 1 [400X, longitudinal section].

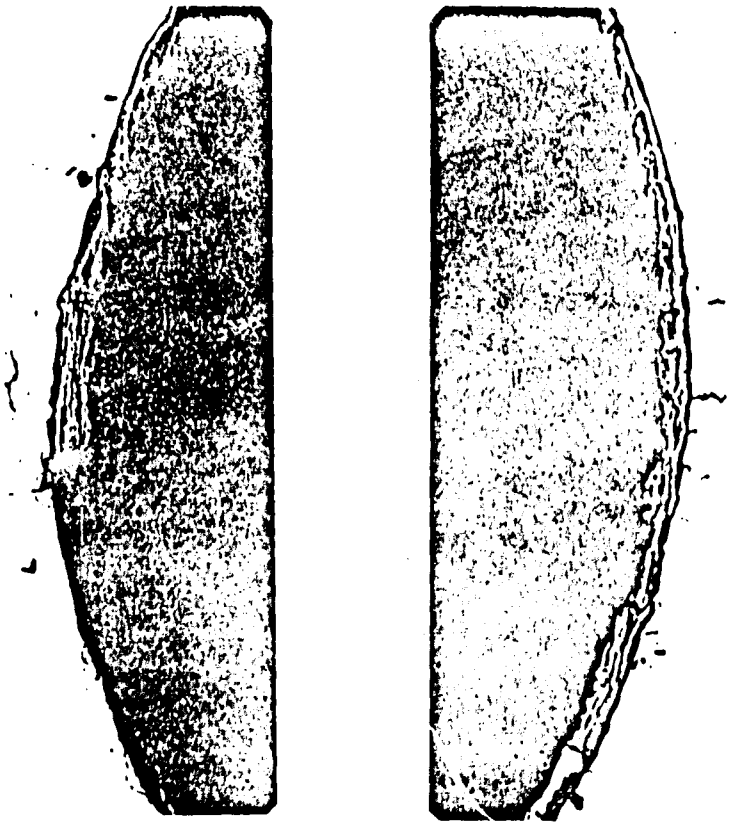

(a)

Left-hand side neighborhood of stress concentration [40X].

(b)

Right-hand side neighborhood of stress concentration [40X].

Fig. 13 Cavitation distribution near the central hole of specimen No. 2.

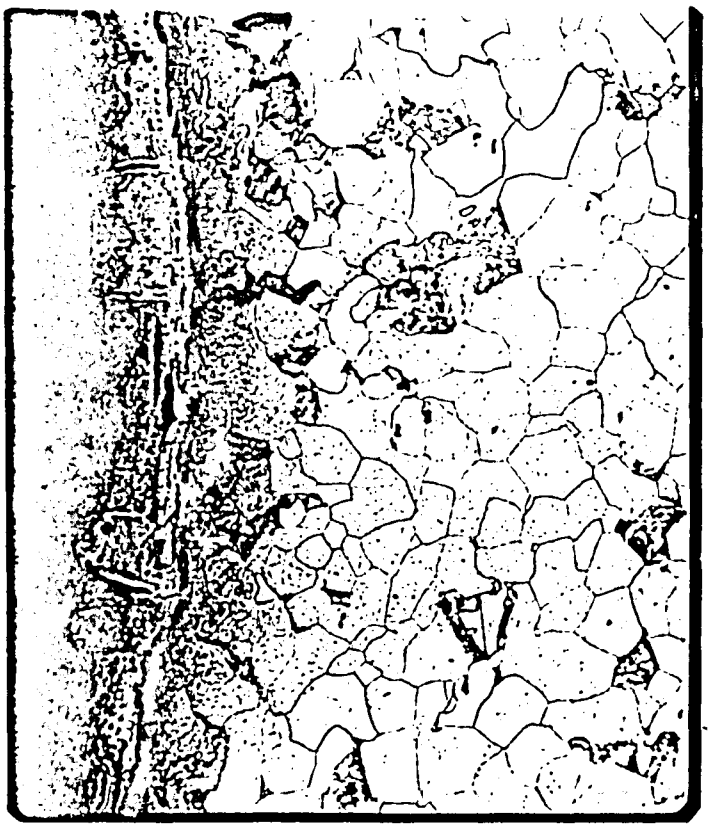

Fig. 14 Magnified etched intergranular cavitation for Fig. 13 (b) [120X].

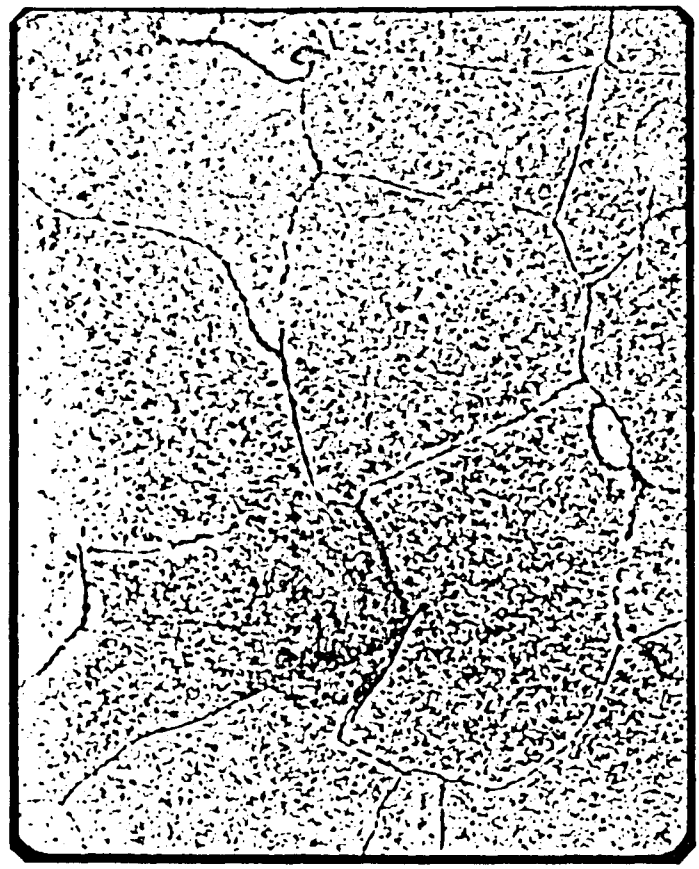

Fig. 15 Etched microstructure for the region far away from the central hole of specimen No. 2 [800X].

REFERENCES

1. R.J. Fields, T. Weerasooriya, and M.F. Ashby, "Fracture Mechanisms in Pure Iron, Two Austenitic, and One Ferritic Steel" Met Trans. (to appear).

2. Code Case N-47-12, Cases of the ASME Boiler and Pressure Vessel Code, American Society of Mechanical Engineers, New York, NY.

3. T.J. Chuang et al., "Non-equilibrium Models for Diffusive Cavitation of Grain Interfaces", Acta Met., Vol. 27, pp. 265-284 (1979).

4. I-W Chen, Creep Cavitation in 304 Stainless Steel, Ph.D. Thesis, M.I.T. (1980).

5. D.R. Hayhurst, "Creep Rupture Under Multiaxial States of Stress", J. Mech. Phys. Solids, Vol. 20, pp. 381-390 (1972).

6. G. Piatti, G. Bernasconi and F.A. Cozzarelli, "Damage Equations for Creep Rapture in Steel", Preceedings of the Fifth International Congress on Structural Mechanics in Reactor Technology (SMIRT), paper no. L 11/4, Berlin.

7. Belloni, G., Bernasconi, G., Piatti, G. "Creep Damage and Rupture in AISI 310 Austenitic Steel", Meccanica, Vol. 12, pp. 84-96 (1977).

8. Matera, R., Piatti, G., Belloni, G., Matteazzi, S., "Danneggiamento a scorrimento viscoso dell'acciaio 2.25 Cr 1 Mo". Proceedings Fourth AIMETA Congress, Florence, 25-28 October, 1978.

9. Robinson, D.N., "A Unified Creep-Plasticity Model for Structural Metals at High Temperatures", ORNL/TM-5969, Oak Ridge National Laboratory, Oct. 1978.

10. Robinson, D.N., "Development of Refined Constitutive Laws" in High-Temperature Structural Design Program Semiannual Prog. Rep. Dec. 31, 1978. ORNL-5540, Oak Ridge National Laboratory, Nov. 1978.

11. Curtis F. Gerald, "Applied Numerical Analysis", Second ed., Addison-Wesley Publishing Company, pp. 250-286.

12. O.C. Zienkiewicz, "The Finite Element Method", 3rd ed., p. 198, McGraw Hill.

13. E. Hinton and J.S. Campbell, "Local and Global Smoothing of Discontinuous Finite Element Functions Using a Least Squares Method", International Journal for Numerical Methods in Engineering, Vol. 8, pp. 461-480 (1974).

VITA

Tai-Sheng Liu was born in Kaohsiung, Taiwan, Republic of China (Free China) on June 21, 1954 to Ms. Lan-Yin Yi and Mr. Yung-Tao Liu. He graduated from National Cheng Kung University in June 1977 with a B.S. degree in Department of Mechanical Engineering, Aeronautical Division.

In September 1979, the author entered the Department of Aerospace Engineering at State University of New York at Buffalo as a graduate student and a teaching assistant. In September 1980, he came to the Department of Mechanical Engineering and Mechanics at Lehigh University. Since then, he worked under Dr. T.J. Delph and Dr. R.J. Fields studying in the field of creep damage in 2 1/4 Cr-1 Mo and 304 stainless steels. He is now a teaching assistant in statics.